

# Scaling properties of a spatial one-particle density-matrix entropy in many-body localized systems

Miroslav Hopjan,<sup>1</sup> Fabian Heidrich-Meisner,<sup>1</sup> and Vincenzo Alba<sup>2</sup>

<sup>1</sup>*Institut für Theoretische Physik, Georg-August-Universität Göttingen,  
Friedrich-Hund-Platz 1, 37077 Göttingen, Germany*

<sup>2</sup>*Institute for Theoretical Physics, Universiteit van Amsterdam,  
Science Park 904, Postbus 94485, 1098 XH Amsterdam, The Netherlands*

We investigate a spatial subsystem entropy extracted from the one-particle density matrix (OPDM) in one-dimensional disordered interacting fermions that host a many-body localized (MBL) phase. Deep in the putative MBL regime, this OPDM entropy exhibits the salient features of localization, despite not being a proper entanglement measure. We numerically show that the OPDM entropy of the eigenstates obeys an area law. Similar to the von-Neumann entropy, the OPDM entropy grows logarithmically with time after a quantum quench, albeit with a different prefactor. Both these features survive at moderately large interactions and well towards the transition into the ergodic phase. The computational cost to calculate the OPDM entropy scales only polynomially with the system size, suggesting that the OPDM provides a promising starting point for developing diagnostic tools for MBL in simulations and experiments.

## I. INTRODUCTION

Many-body localized (MBL) systems challenge the usual paradigm of thermalization [1–5]. While it is well-established that for non-interacting particles, disorder leads to Anderson localization [6], it has been suggested that for sufficiently strong disorder, a localized phase survives in the presence of interactions [7, 8]. Despite intense theoretical effort (see recent reviews [1–5]), the scenario is not fully settled. On the experimental side, MBL has been investigated in trapped ions [9], ultra-cold atoms [10–14] or superconducting qubits [15–18]. Experimental signatures of MBL have been observed in the quasiperiodic Aubry-André Fermi-Hubbard model [11, 19], the disordered Ising model [9], the disordered Bose-Hubbard model (BHM) [10, 14] and the quasiperiodic Aubry-André Bose-Hubbard model [12, 13].

Entanglement-related measures, such as the von-Neumann entropy, display several intriguing behaviours in the putative MBL phase. First, a distinctive feature of localization is that eigenstates exhibit area-law entanglement [20–22], in stark contrast with the volume law expected in clean systems. Second, the entanglement entropy grows logarithmically after global quenches [23–25], which is regarded as a “smoking gun” evidence for MBL. Indeed, this is different in Anderson-localized systems, where the entanglement entropy saturates, and in clean systems, different from, for instance, integrable ones, where a linear behaviour is rigorously established [26–29]. The logarithmic growth can be explained by the existence of emergent local integrals of motion in the MBL phase [25, 30–32]. Remarkably, the logarithmic growth of the entanglement entropy has been observed in cold-atom experiments [13] and systems of superconducting qubits [15, 17]. However, measuring entanglement is a challenging task and cannot easily be scaled up to larger systems, as it requires full quantum state tomography [15], accessing all the  $n$ -point correlation functions

[13, 17], or a high-fidelity state preparation [13].

Here, we show that a suitably defined spatial-subsystem entropy based on the *one-particle density matrix* (OPDM) computed in eigenstates and its out-of-equilibrium dynamics after a quantum quench contain salient information about MBL phases, akin to the behavior of the spatial entanglement entropy. The main motivation for studying the OPDM is that in the MBL phase, the eigenstates of the OPDM are localized in real space but delocalized in the ergodic phase [33, 34]. Moreover, its eigenvalues indicate Fock-space localization in MBL regime [33, 34], a defining feature of MBL [8, 35–37]. This is reflected in the OPDM being close to that of a free-fermion system [33, 34, 38–42], and its eigenmodes being a proxy for the localized quasiparticles [34].

We focus on the OPDM restricted to a subsystem  $A$  and on the associated entropy. For non-interacting fermionic systems, this coincides with the von-Neumann entropy [43, 44]. We consider a generic model of disordered spinless fermions with nearest-neighbor interactions. Numerically, we show that in the MBL phase, the disorder-averaged OPDM entropy exhibits an area law, similar to the von-Neumann entropy. This is remarkable because in the presence of interactions, the OPDM entropy is not a proper (spatial) entanglement measure.

Crucially, after a quantum quench in the MBL phase, the OPDM entropy increases logarithmically with time, similar to the von-Neumann entropy. The prefactor of the logarithmic growth is non-universal, and it is different from that of the von-Neumann entropy. The logarithmic growth survives for moderately strong interactions and as the disorder strength is decreased. In the non-interacting limit, i.e., for the Anderson insulator, the OPDM entropy saturates. Our results establish the OPDM entropy as an alternative diagnostic tool for the MBL phase. This could be relevant for both experiments and approximate theoretical approaches inspired by ab-initio methods. Importantly, the computational cost of extracting the OPDM entropy from the correlation function is only polynomial.

We also note that the OPDM diagnostic tool that we propose is not limited to the regime of weak interactions, in contrast with other one-body measures based on Anderson orbitals [45] or the self-consistent Hartree-Fock approximation [46].

## II. ENTROPY OF THE ONE-PARTICLE DENSITY MATRIX

In this paper, we consider spinless fermions with a nearest-neighbor interaction and with diagonal disorder described by the Hamiltonian

$$H = \sum_{i=1}^L \left[ -\frac{J}{2}(c_i^\dagger c_{i+1} + h.c.) + V(n_i - 1/2)(n_{i+1} - 1/2) + \epsilon_i(n_i - 1/2) \right], \quad (1)$$

where  $c_i^{(\dagger)}$  is a fermionic creation/annihilation operator and  $n_i = c_i^\dagger c_i$  is the fermionic density at site  $i$ .  $L$  is the system size,  $J$  is the hopping matrix element,  $V$  is the strength of the nearest-neighbor interactions, and  $\epsilon_i$  is a random potential drawn from a uniform box distribution  $[-W, W]$ . Using a Jordan-Wigner transformation, Eq. (1) can be mapped onto a spin-1/2 XXZ chain with random local magnetic field. For  $V/J = 1$ , one obtains the isotropic Heisenberg model which is a standard system where MBL physics has been investigated [5, 35]. Here, we consider  $V/J = 1$  and  $V/J = 0.1$  as representative of the strong and weak interactions regime, respectively.

We will compare the behavior of the OPDM entropy to that of the von-Neumann entanglement entropy  $S$  of a subsystem  $A$ . First, we split the system into two parts,  $A$  and its complement  $\bar{A}$ . We always consider the case in which  $A$  and  $\bar{A}$  are equal to the half chain. Any state of the full system  $|\psi\rangle$  can be Schmidt-decomposed as

$$|\psi\rangle = \sum_i \sqrt{\lambda_i} |\phi_i\rangle_A |\varphi_i\rangle_B, \quad (2)$$

where the  $\sqrt{\lambda_i}$  are the Schmidt coefficients and  $\{|\phi_i\rangle_A\}$  and  $\{|\varphi_i\rangle_{\bar{A}}\}$  are orthonormal bases for  $A$  and  $\bar{A}$ . The von-Neumann entanglement entropy is given by

$$S_{\text{vN}} = - \sum_i \lambda_i \ln \lambda_i. \quad (3)$$

For a pure state  $|\psi\rangle$ , Eq. (2) implies that  $S_{\text{vN}}(A) = S_{\text{vN}}(\bar{A})$ .

Our main interest is in the properties of an entropy extracted from the one-particle density matrix (OPDM): We restrict the OPDM  $\rho_{ij}^{(1)} = \langle \psi | c_i^\dagger c_j | \psi \rangle$  ( $1 \leq i, j \leq L$ ) to a subsystem  $A$ , which yields

$$C_{ij}^{(A)} = \langle \psi | c_i^\dagger c_j | \psi \rangle, \quad i, j \in A, \quad (4)$$

where  $|\psi\rangle$  is a many-body state.  $C_{ij}^{(A)}$  is usually called correlation matrix. Given the eigenvalues  $n_\alpha$  of  $C_{ij}^{(A)}$ , we define the OPDM entropy as

$$S_{\text{OPDM}}(A) = - \sum_\alpha (n_\alpha \ln(n_\alpha) + (1 - n_\alpha) \ln(1 - n_\alpha)). \quad (5)$$

Even though we restricted the OPDM to a subsystem, we use the name OPDM entropy for simplicity. The OPDM entropy defined here should not be confused with the entanglement of one particle with all other ones [33, 34, 47] (this is the residual entropy defined in [48]). For non-interacting fermions,  $S_{\text{OPDM}}$  coincides with the von-Neumann entropy [43, 44].

Several remarks are in order. First, an important remark is that for free-fermion systems, if  $A$  is the full system, the eigenvalues  $n_\alpha$  are the fermionic occupations of the single-particle orbitals and  $n_\alpha = 0, 1$ , with  $\sum_\alpha n_\alpha = N$ , where  $N$  the total number of fermions. By using (5), this implies that the full-system entanglement entropy is zero. In the presence of interactions, this is not the case for the OPDM entropy. Specifically, upon switching interactions on, yet still in the MBL regime, the eigenvalues of the OPDM exhibit a bimodal distribution with  $n_\alpha \approx 0, 1$ , signaling that the true eigenmodes are quasiparticles. Note that this implies that the full system OPDM entropy is non-zero except in trivial limiting cases [see the additional discussion in the Supplemental Material (SM)[48]]. Interestingly, this suggests that the OPDM entropy provides an upper bound for the entanglement entropy. We observe that this remains true also if  $A$  is not the full system, i.e.,  $S_{\text{OPDM}}(A) \geq S_{\text{vN}}(A)$ .

Another important observation is that in the presence of interactions,  $S_{\text{OPDM}}(A) \neq S_{\text{OPDM}}(\bar{A})$ . For this reason, we introduce  $S_{\text{OPDM}}^{\text{min}}$  as

$$S_{\text{OPDM}}^{\text{min}} = \min(S_{\text{OPDM}}(A), S_{\text{OPDM}}(\bar{A})). \quad (6)$$

Both  $S_{\text{OPDM}}^{\text{min}}$  and a complementary  $S_{\text{OPDM}}^{\text{max}}$  display similar behaviour with  $S_{\text{OPDM}}^{\text{min}}$  being superior to  $S_{\text{OPDM}}^{\text{max}}$  [see [48]]. In the rest of the paper, we focus on  $S_{\text{OPDM}}^{\text{min}}$ .

In the following sections, we show that the OPDM entropy exhibits two of the hallmark features of MBL, namely the area-law behaviour in the excited states and the logarithmic spreading after a global quantum quench. This can be understood in the limit of strong disorder, i.e., deep in the MBL phase. In this limit, the eigenvalues of the OPDM take the values  $n_\alpha = 0, 1$ , i.e., they exhibit the typical step-like behaviour as for free-fermion systems. This signals that the MBL-localized state is close to a single Slater determinant [33, 34], for which the OPDM entropy coincides with the von-Neumann one. Since this proximity to a Slater determinant persists throughout the MBL regime, it is natural to expect that for sufficiently strong disorder, the OPDM entropy (5) exhibits a similar behaviour as the von-Neumann entropy.

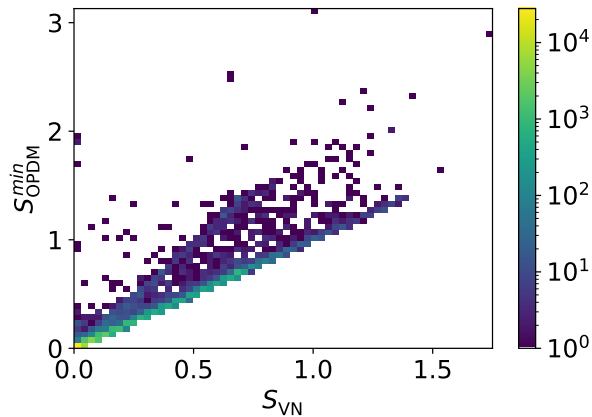


FIG. 1. 2D histogram showing the correlation between von-Neumann entanglement entropy  $S_{\text{vN}}$  and the OPDM entropy  $S_{\text{OPDM}}^{\text{min}}$ , both computed in the same eigenstate. For each value of  $S_{\text{vN}}$ , the color encodes the number of eigenstates with that entropy. The  $y$ -axis shows the corresponding OPDM entropy. Data are averaged over  $10^4$  disorder realization and are obtained from  $6 \cdot 10^4$  eigenstates. Results are for fixed  $\epsilon = 1$ ,  $V/J = 1$ ,  $W/J = 15$ , and system size  $L = 16$ .

### III. AREA LAW OF THE OPDM ENTROPY IN THE MBL REGIME

In this section, we show that for the eigenstates of (1), the disorder-averaged OPDM entropy defined in Eq. (6) satisfies the area law. We use exact diagonalization to compute all the eigenstates of (1) up to  $L = 18$ . We consider a system with periodic boundary conditions, and we restrict ourselves to a fixed number of fermions  $N/L = 1/2$ , which corresponds to zero magnetization in the spin language. We average the OPDM entropy over  $10^4$  disorder realizations for  $L \leq 16$  and  $10^3$  disorder realizations for  $L = 18$ . We focus on entanglement properties of mid-spectrum eigenstates. Precisely, for each disorder realization, we consider eigenstates with an energy such that  $(E - E_{\text{min}})/(E_{\text{max}} - E_{\text{min}}) \approx 1/2$ , with  $E_{\text{min}}$  the ground-state energy and  $E_{\text{max}}$  the energy of the most excited state. We use the shift-and-invert method [49] to target the desired energy window. Typically, for each disorder realization, we consider 10 eigenstate.

In Fig. 1, we focus on the half-chain entanglement entropy and OPDM entropy for a system with  $L = 16$ . Results are for  $V/J = 1$  and  $W/J = 15$ . For these parameters, the system is expected to be in the MBL phase because the putative transition happens at  $W_c/J \approx 4$  [33, 35, 50–52]. Note also that for  $V/J = 1$ , the system is far from the “trivial” non-interacting limit  $V = 0$ . The histogram shows the correlation between  $S_{\text{vN}}$  (on the  $x$ -axis) and  $S_{\text{OPDM}}$  computed in the same eigenstate. The color scale denotes the number of eigenstates with a given value of the entanglement entropy. The  $y$ -axis shows the corresponding value of the OPDM entropy.

The main conclusion from Fig. 1 is that the OPDM

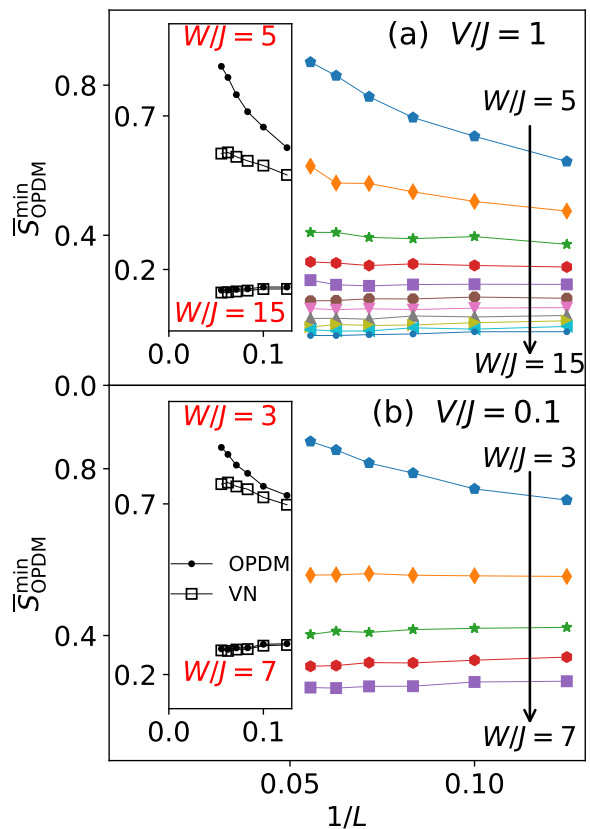


FIG. 2. (a): Main panel: Disorder average of the OPDM entropy  $\bar{S}_{\text{OPDM}}^{\text{min}}$  plotted as a function of  $L$  for  $V/J = 1$  and disorder strength  $W/J = 5, \dots, 15$  (different symbols). The arrow shows increasing disorder strength. Inset: Comparison between OPDM entropy  $\bar{S}_{\text{OPDM}}^{\text{min}}$  (full circles) and von-Neumann entropy  $\bar{S}_{\text{vN}}$  (open squares) for  $V/J = 1$  and  $W/J = 5, 15$ . (b): Same as in (a) for  $1/L$  for weak interactions  $V/J = 0.1$  and disorder strength  $W/J = 3, \dots, 7$ .

entropy is always larger than the entanglement entropy, i.e.,  $S_{\text{vN}} \leq S_{\text{OPDM}}^{\text{min}}$  for all eigenstates. We have verified, up to machine precision, that this is true for all our data. One can also observe that the majority of the points lies close to the diagonal, i.e., for most of the eigenstates,  $S_{\text{vN}}$  is close to  $S_{\text{OPDM}}^{\text{min}}$ . Interestingly, a second cluster of states is visible at  $S_{\text{OPDM}}^{\text{min}} = 2S_{\text{vN}}$ . With increasing disorder strength, at least for fixed system size, all eigenstates collapse on the main diagonal and the OPDM entropy becomes the same as the von-Neumann entropy.

We now demonstrate that the *disorder-averaged* OPDM entropy  $\bar{S}_{\text{OPDM}}^{\text{min}}$  obeys the area law. In Fig. 2, we present the average OPDM entropy for the half chain as a function of  $L$  for several values of  $W/J$  and for  $V/J = 1$  and for  $V/J = 0.1$ . For  $V/J = 1$ , standard diagnostic tools give a putative MBL transition at  $W/J \approx 4$  [33, 35, 50–52] (see also [53–63]). In Fig. 2(a), we display the  $L$ -dependence of the OPDM entropy on the MBL side. Deep in the MBL phase (for instance, for  $W/J \geq 10$ ), the OPDM entropy is almost  $L$ -independent,

implying area-law behaviour [20–22]. Moreover, the OPDM entropy becomes very close to the von-Neumann entropy upon increasing the disorder strength (see the inset of Fig. 2(a)). For the regime of weak interactions  $V/J = 0.1$  (see Fig. 2(b)), smaller values of  $W$  are sufficient to observe the area-law behaviour. This is expected because upon lowering  $V$ , the MBL transition is shifted towards smaller values of  $W$ . We estimate the transition at  $V = 0.1J$  from standard diagnostic tools, such as the average gap ratio [35, 64], or the occupation distance measure [52], which give  $W_c/J \approx 2 - 3$  [see the SM [48]].

#### IV. LOGARITHMIC GROWTH OF THE OPDM ENTROPY IN THE MBL REGIME

Next, we discuss the spreading of the OPDM entropy after a global quantum quench deep in the MBL phase. We consider the evolution from initial random product states such as  $|\psi_0\rangle = |1010\dots 1\rangle$ , where 0,1 are the initial fermionic occupations. We study the Hamiltonian dynamics  $|\psi(t)\rangle = e^{-iHt}|\psi_0\rangle$  by using full exact diagonalization of  $H$ . For each disorder configuration, we select product states  $|\psi_0\rangle$  with energy density  $\epsilon_0 = 1/2 - |(\langle\psi_0|H|\psi_0\rangle - E_{\min})/(E_{\max} - E_{\min})| \lesssim 2 \cdot 10^{-4}$ , i.e., close to mid-spectrum energy density. We average over 200 disorder realizations.

In the putative MBL phase, the von-Neumann entropy grows logarithmically after global quenches [23–25, 65], whereas on the ergodic side, a ballistic or sub-ballistic entanglement growth is observed [66]. The change of behaviour happens at the eigenstate transition [65].

In Fig. 3(a), we show the dynamics of the OPDM entropy for  $V/J = 1$  (strong interactions) and for  $W/J = 5, \dots, 15$  and for  $V/J = 0.1$  and  $W/J = 3, \dots, 7$  (weak interactions). In both cases, the system is in the MBL phase. For large enough times, the data exhibit a clear logarithmic increase for all the values of  $W$ . The prefactor of the logarithmic growth depends on the interaction strength  $V$ , and hence is non-universal, as for the von-Neumann entropy. Note that in the limit  $W \rightarrow \infty$ , the entropy saturates. Interestingly, the prefactors of the logarithmic growth of the OPDM entropy and of the von-Neumann entropy are not the same. This is illustrated in the insets of Fig. 3. Only in the limit of large  $W/J$ , the dynamics of the OPDM entropy becomes quantitatively the same as the von-Neumann entropy, reflecting that the full system is described by a single Slater determinant.

Finally, several interesting features appear for weak interactions (see Fig. 3 (b)). First, longer times are needed for the logarithmic behaviour to set in. For instance, for  $V/J = 0.1$ , this happens for  $tJ \geq 100$ . Moreover, the dynamics of the OPDM entropy and that of the von-Neumann entropy is the same at short times. This is highlighted in the insets in Fig. 3. Clearly, the OPDM entropy coincides with the von-Neumann entropy up to  $tJ \approx 10$ .

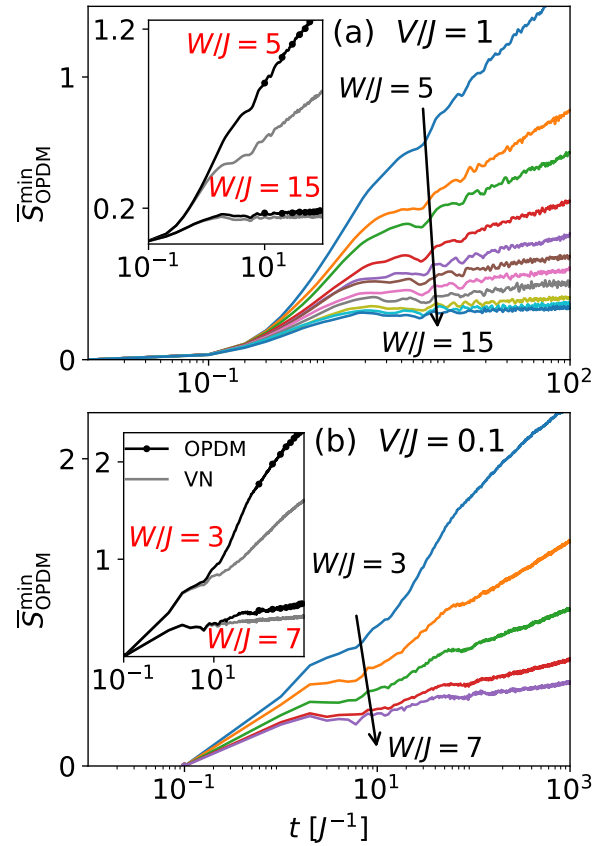


FIG. 3. (a): Main panel: Time evolution of the average OPDM entropy  $\bar{S}_{\text{OPDM}}^{\text{min}}$  for  $L = 16$ ,  $V/J = 1$  and disorder strength  $W/J = 5 - 15$ . The arrow denotes increasing disorder strength. For all values of  $W$ , a clear logarithmic growth with a non-universal prefactor is visible at long times. Inset: Comparison between the OPDM entropy  $\bar{S}_{\text{OPDM}}^{\text{min}}$  (full circles) and the von-Neumann entropy  $\bar{S}_{\text{VN}}$  (gray lines) for  $L = 16$ ,  $V/J = 1$  and  $W/J = 5, 15$ . (b) Same as in (a) for weak interactions  $V/J = 0.1$ .

#### V. CONCLUSIONS

We provided numerical evidence that the OPDM entropy exhibits the salient features of the von-Neumann entropy in putative MBL phases of matter. Specifically, deep in MBL phases, the eigenstates OPDM entropy obeys the area law. Most importantly, the entropy grows logarithmically after a global quantum quench. Although formally, this is expected in the limit  $W/J \rightarrow \infty$ , we observe that there is a sizeable region in parameter space, i.e., interaction and disorder strength, where this behavior persists.

There are several interesting directions for future work. First, our results could be combined with *ab-initio* methods for the correlation functions, e.g., Green's function methods [46, 67, 68]. This would allow to compute the evolution of the OPDM entropy for larger systems, and also in higher dimensions. Moreover, it would be interesting to measure the evolution of the OPDM en-



trophy in cold-atom experiments using single-site resolution [13, 69] or in embryonic quantum computers. Finally, in contrast with the entanglement entropy, the OPDM entropy relies on the fermionic correlation functions, which are standard tools in condensed matter physics. This renders the OPDM amenable to analytical study and, for instance, by using the techniques of

Ref. 1.

## ACKNOWLEDGMENTS

We acknowledge useful discussions with J. H. Bardarson.

- 
- [1] E. Altman and R. Vosk, *Ann. Rev. Cond. Matt. Phys.* **6**, 383 (2015).
  - [2] R. Nandkishore and D. A. Huse, *Ann. Rev. Cond. Matt. Phys.* **6**, 15 (2015).
  - [3] E. Altman, *Nat. Phys.* **14**, 979 (2018).
  - [4] F. Alet and N. Laflorencie, *C. R. Phys.* **19**, 498 (2018).
  - [5] D. A. Abanin, E. Altman, I. Bloch, and M. Serbyn, *Rev. Mod. Phys.* **91**, 021001 (2019).
  - [6] P. W. Anderson, *Phys. Rev.* **109**, 1492 (1958).
  - [7] I. V. Gornyi, A. D. Mirlin, and D. G. Polyakov, *Phys. Rev. Lett.* **95**, 206603 (2005).
  - [8] D. Basko, I. Aleiner, and B. Altshuler, *Ann. Phys. (N.Y.)* **321**, 1126 (2006).
  - [9] J. Smith, A. Lee, P. Richerme, B. Neyenhuis, P. W. Hess, P. Hauke, M. Heyl, D. A. Huse, and C. Monroe, *Nat. Phys.* **12**, 907 (2016).
  - [10] J.-Y. Choi, S. Hild, J. Zeiher, P. Schauß, A. Rubio-Abadal, T. Yefsah, V. Khemani, D. A. Huse, I. Bloch, and C. Gross, *Science* **352**, 1547 (2016).
  - [11] M. Schreiber, S. S. Hodgman, P. Bordia, H. P. Lüschen, M. H. Fischer, R. Vosk, E. Altman, U. Schneider, and I. Bloch, *Science* **349**, 842 (2015).
  - [12] M. Rispoli, A. Lukin, R. Schittko, S. Kim, M. E. Tai, J. Léonard, and M. Greiner, *Nature* **573**, 385 (2019).
  - [13] A. Lukin, M. Rispoli, R. Schittko, M. E. Tai, A. M. Kaufman, S. Choi, V. Khemani, J. Léonard, and M. Greiner, *Science* **364**, 256 (2019).
  - [14] A. Rubio-Abadal, J.-Y. Choi, J. Zeiher, S. Hollerith, J. Rui, I. Bloch, and C. Gross, *Phys. Rev. X* **9**, 041014 (2019).
  - [15] K. Xu, J.-J. Chen, Y. Zeng, Y.-R. Zhang, C. Song, W. Liu, Q. Guo, P. Zhang, D. Xu, H. Deng, K. Huang, H. Wang, X. Zhu, D. Zheng, and H. Fan, *Phys. Rev. Lett.* **120**, 050507 (2018).
  - [16] P. Roushan, C. Neill, J. Tangpanitanon, V. M. Bastidas, A. Megrant, R. Barends, Y. Chen, Z. Chen, B. Chiaro, A. Dunsworth, A. Fowler, B. Foxen, M. Giustina, E. Jeffrey, J. Kelly, E. Lucero, J. Mutus, M. Neeley, C. Quintana, D. Sank, A. Vainsencher, J. Wenner, T. White, H. Neven, D. G. Angelakis, and J. Martinis, *Science* **358**, 1175 (2017).
  - [17] B. Chiaro, C. Neill, A. Bohrdt, M. Filippone, F. Arute, K. Arya, R. Babbush, D. Bacon, J. Bardin, R. Barends, S. Boixo, D. Buell, B. Burkett, Y. Chen, Z. Chen, R. Collins, A. Dunsworth, E. Farhi, A. Fowler, B. Foxen, C. Gidney, M. Giustina, M. Harrigan, T. Huang, S. Isakov, E. Jeffrey, Z. Jiang, D. Kafri, K. Kechedzhi, J. Kelly, P. Klimov, A. Korotkov, F. Kostritsa, D. Landhuis, E. Lucero, J. McClean, X. Mi, A. Megrant, M. Mohseni, J. Mutus, M. McEwen, O. Naaman, M. Neeley, M. Niu, A. Petukhov, C. Quintana, N. Rubin, D. Sank, K. Satzinger, A. Vainsencher, T. White, Z. Yao, P. Yeh, A. Zalcman, V. Smelyanskiy, H. Neven, S. Gopalakrishnan, D. Abanin, M. Knap, J. Martinis, and P. Roushan, *arXiv:1910.06024*.
  - [18] Q. Guo, C. Cheng, Z.-H. Sun, Z. Song, H. Li, Z. Wang, W. Ren, H. Dong, D. Zheng, Y.-R. Zhang, R. Mondaini, H. Fan, and H. Wang, *Nat. Phys.* (2020), 10.1038/s41567-020-1035-1.
  - [19] T. Kohlert, S. Scherg, X. Li, H. P. Lüschen, S. Das Sarma, I. Bloch, and M. Aidelsburger, *Phys. Rev. Lett.* **122**, 170403 (2019).
  - [20] B. Bauer and C. Nayak, *J. Stat. Mech. Theor. Exp.* **2013**, P09005 (2013).
  - [21] J. A. Kjäll, J. H. Bardarson, and F. Pollmann, *Phys. Rev. Lett.* **113**, 107204 (2014).
  - [22] M. Friesdorf, A. H. Werner, W. Brown, V. B. Scholz, and J. Eisert, *Phys. Rev. Lett.* **114**, 170505 (2015).
  - [23] M. Žnidarič, T. Prosen, and P. Prelovšek, *Phys. Rev. B* **77**, 064426 (2008).
  - [24] J. H. Bardarson, F. Pollmann, and J. E. Moore, *Phys. Rev. Lett.* **109**, 017202 (2012).
  - [25] M. Serbyn, Z. Papić, and D. A. Abanin, *Phys. Rev. Lett.* **110**, 260601 (2013).
  - [26] P. Calabrese and J. Cardy, *Journal of Statistical Mechanics: Theory and Experiment* **2005**, P04010 (2005).
  - [27] G. D. Chiara, S. Montangero, P. Calabrese, and R. Fazio, *Journal of Statistical Mechanics: Theory and Experiment* **2006**, P03001 (2006).
  - [28] M. Fagotti and P. Calabrese, *Phys. Rev. A* **78**, 010306 (2008).
  - [29] V. Alba and P. Calabrese, *Proceedings of the National Academy of Sciences* **114**, 7947 (2017).
  - [30] D. A. Huse, R. Nandkishore, and V. Oganesyan, *Phys. Rev. B* **90**, 174202 (2014).
  - [31] J. Z. Imbrie, V. Ros, and A. Scardicchio, *Ann. Phys. (Leipzig)* **529**, 1600278 (2017).
  - [32] J. Z. Imbrie, *Phys. Rev. Lett.* **117**, 027201 (2016).
  - [33] S. Bera, H. Schomerus, F. Heidrich-Meisner, and J. H. Bardarson, *Phys. Rev. Lett.* **115**, 046603 (2015).
  - [34] S. Bera, T. Martynek, H. Schomerus, F. Heidrich-Meisner, and J. H. Bardarson, *Ann. Phys. (Leipzig)* **529**, 1600356 (2017).
  - [35] D. J. Luitz, N. Laflorencie, and F. Alet, *Phys. Rev. B* **91**, 081103 (2015).
  - [36] S. Roy, J. T. Chalker, and D. E. Logan, *Phys. Rev. B* **99**, 104206 (2019).
  - [37] D. E. Logan and S. Welsh, *Phys. Rev. B* **99**, 045131 (2019).
  - [38] T. L. M. Lezama, S. Bera, H. Schomerus, F. Heidrich-Meisner, and J. H. Bardarson, *Phys. Rev. B* **96**, 060202 (2017).
  - [39] S.-H. Lin, B. Sbierski, F. Dorfner, C. Karrasch, and F. Heidrich-Meisner, *SciPost Phys.* **4**, 002 (2018).

- [40] W. Buijsman, V. Gritsev, and V. Cheianov, *SciPost Phys.* **4**, 38 (2018).
- [41] B. Villalonga, X. Yu, D. J. Luitz, and B. K. Clark, *Phys. Rev. B* **97**, 104406 (2018).
- [42] C. P. Chen, M. Szyniszewski, and H. Schomerus, *Phys. Rev. Research* **2**, 023118 (2020).
- [43] I. Peschel and V. Eisler, *Journal of Physics A: Mathematical and Theoretical* **42**, 504003 (2009).
- [44] J. I. Latorre and A. Riera, *Journal of Physics A: Mathematical and Theoretical* **42**, 504002 (2009).
- [45] G. De Tomasi, F. Pollmann, and M. Heyl, *Phys. Rev. B* **99**, 241114 (2019).
- [46] S. A. Weidinger, S. Gopalakrishnan, and M. Knap, *Phys. Rev. B* **98**, 224205 (2018).
- [47] G. De Tomasi, S. Bera, J. H. Bardarson, and F. Pollmann, *Phys. Rev. Lett.* **118**, 016804 (2017).
- [48] See Supplemental Material at [URL will be inserted by publisher] for details.
- [49] F. Pietracaprina, N. Macé, D. J. Luitz, and F. Alet, *SciPost Phys.* **5**, 45 (2018).
- [50] N. Macé, F. Alet, and N. Laflorencie, *Phys. Rev. Lett.* **123**, 180601 (2019).
- [51] N. Laflorencie, G. Lemarié, and N. Macé, *arXiv:2004.02861*.
- [52] M. Hopjan and F. Heidrich-Meisner, *Phys. Rev. A* **101**, 063617 (2020).
- [53] T. Devakul and R. R. P. Singh, *Phys. Rev. Lett.* **115**, 187201 (2015).
- [54] E. V. H. Doggen, F. Schindler, K. S. Tikhonov, A. D. Mirlin, T. Neupert, D. G. Polyakov, and I. V. Gornyi, *Phys. Rev. B* **98**, 174202 (2018).
- [55] T. Chanda, P. Sierant, and J. Zakrzewski, *Phys. Rev. B* **101**, 035148 (2020).
- [56] V. Khemani, D. N. Sheng, and D. A. Huse, *Phys. Rev. Lett.* **119**, 075702 (2017).
- [57] J. Šuntajs, J. Bonča, T. Prosen, and L. Vidmar, *arXiv:1905.06345*.
- [58] P. Sierant, D. Delande, and J. Zakrzewski, *Phys. Rev. Lett.* **124**, 186601 (2020).
- [59] D. A. Abanin, J. H. Bardarson, G. De Tomasi, S. Gopalakrishnan, V. Khemani, S. A. Parameswaran, F. Pollmann, A. C. Potter, M. Serbyn, and R. Vasseur, *arXiv:1911.04501*.
- [60] R. K. Panda, A. Scardicchio, M. Schulz, S. R. Taylor, and M. Žnidarič, *EPL* **128**, 67003 (2019).
- [61] T. Chanda, P. Sierant, and J. Zakrzewski, *Phys. Rev. Research* **2**, 032045 (2020).
- [62] J. Šuntajs, J. Bonča, T. Prosen, and L. Vidmar, *Phys. Rev. B* **102**, 064207 (2020).
- [63] P. Sierant, M. Lewenstein, and J. Zakrzewski, *Phys. Rev. Lett.* **125**, 156601 (2020).
- [64] V. Oganesyan and D. A. Huse, *Phys. Rev. B* **75**, 155111 (2007).
- [65] M. Serbyn, Z. Papić, and D. A. Abanin, *Phys. Rev. X* **5**, 041047 (2015).
- [66] D. J. Luitz, N. Laflorencie, and F. Alet, *Phys. Rev. B* **93**, 060201 (2016).
- [67] Y. Bar Lev and D. R. Reichman, *Phys. Rev. B* **89**, 220201 (2014).
- [68] Y. B. Lev and D. R. Reichman, *EPL (Europhysics Letters)* **113**, 46001 (2016).
- [69] J. F. Sherson, C. Weitenberg, M. Endres, M. Cheneau, I. Bloch, and S. Kuhr, *Nature* **467**, 68 (2010).
- [70] L. D'Alessio, Y. Kafri, A. Polkovnikov, and M. Rigol, *Adv. Phys.* **65**, 239 (2016).
- [71] A. B. Harris, *Journal of Physics C: Solid State Physics* **7**, 1671 (1974).
- [72] A. Chandran, C. R. Laumann, and V. Oganesyan, *arXiv:1509.04285*.

## SUPPLEMENTAL MATERIAL: SCALING PROPERTIES OF A SPATIAL OPDM ENTROPY IN MBL SYSTEMS

In this Supplemental Material, we discuss the finite-size scaling of  $\bar{S}_{\text{OPDM}}^{\text{max}}$  in the putative MBL phase. Furthermore, we numerically show that  $\bar{S}_{\text{OPDM}}^{\text{max}}$  grows logarithmically with time after a global quench, similar to  $\bar{S}_{\text{OPDM}}^{\text{min}}$ . Interestingly, the logarithmic growth is also visible in the OPDM entropy. Finally, we estimate the location of the putative ergodic-MBL transition for  $V/J = 0.1$ .

### S1. FINITE-SIZE SCALING OF $\bar{S}_{\text{OPDM}}^{\text{max}}$ IN THE LOCALIZED PHASE

In the main text, we focus on the properties of the OPDM entropy  $S_{\text{OPDM}}^{\text{min}}$ . Here, we discuss  $S_{\text{OPDM}}^{\text{max}}$  which is defined as  $S_{\text{OPDM}}^{\text{max}} = \max(S_{\text{OPDM}}(A), S_{\text{OPDM}}(\bar{A}))$ , with  $\bar{A}$  the complement of  $A$ . Note that from the analysis performed in the main text, one has the inequalities

$$\bar{S}_{\text{vN}} \leq \bar{S}_{\text{OPDM}}^{\text{min}} \leq \bar{S}_{\text{OPDM}}^{\text{max}}. \quad (\text{S.1})$$

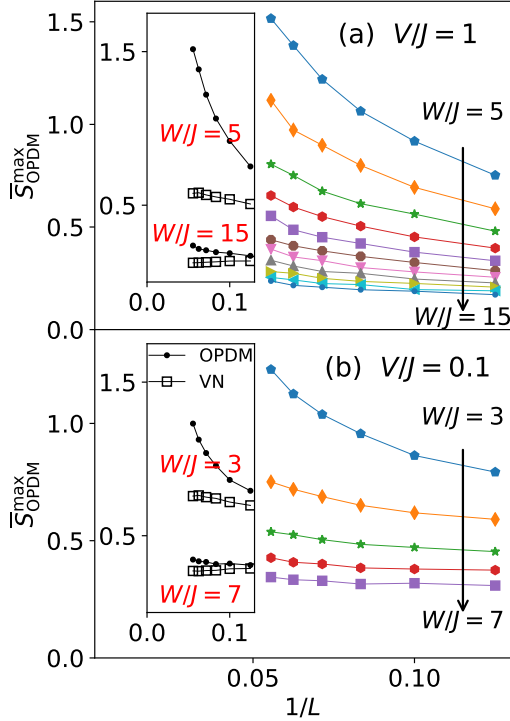


FIG. S1. (a): Main panel: Disorder average of the OPDM entropy  $\bar{S}_{\text{OPDM}}^{\text{max}}$  plotted as a function of  $L$  for  $V/J = 1$  and disorder strength  $W/J = 5, \dots, 15$  (different symbols). The arrow shows increasing disorder strength. Inset: Comparison between  $\bar{S}_{\text{OPDM}}^{\text{max}}$  (full circles) and von-Neumann entropy  $\bar{S}_{\text{vN}}$  (open squares) for  $V/J = 1$  and  $W/J = 5, 15$ . (b): Same as in (a) for weak interactions  $V/J = 0.1$  and disorder strength  $W/J = 3, \dots, 7$ .

In Fig. 2, we show the average OPDM entropy  $\bar{S}_{\text{OPDM}}^{\text{max}}$  for the half chain as a function of  $L$  and for several values of disorder strength  $W/J$ . As in the main text, we show results for  $V/J = 1$  and for  $V/J = 0.1$ .

We observe that deep in the MBL phase, e.g., at  $W/J \approx 15$  for  $V/J = 1$  [see Fig. S1(a)], the behaviour is similar to that of  $\bar{S}_{\text{OPDM}}^{\text{min}}$  (see Fig. 2 in the main text). The data are compatible with the area-law scaling  $\bar{S}_{\text{OPDM}}^{\text{max}} \rightarrow c$  for  $L \rightarrow \infty$ , with  $c$  an  $L$ -independent constant, although the numerical evidence is weaker than for  $\bar{S}_{\text{OPDM}}^{\text{min}}$ . The system sizes accessible with our numerics do not allow us to make any conclusive statement.

### S2. DYNAMICS OF $\bar{S}_{\text{OPDM}}^{\text{max}}$

Here, we provide robust numerical evidence that  $\bar{S}_{\text{OPDM}}^{\text{max}}$  grows logarithmic with time after a global quantum quench in the MBL phase as well. In Fig. S2, we show  $\bar{S}_{\text{OPDM}}^{\text{max}}$  for  $V/J = 1$  (strong interactions) plotted versus time. We display results for  $V/J = 1$  (strong inter-

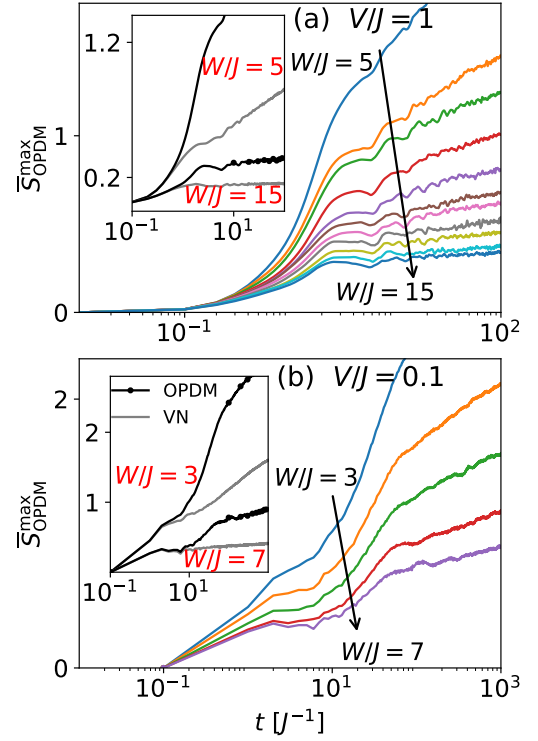


FIG. S2. (a): Main panel: Time evolution of the average OPDM entropy  $\bar{S}_{\text{OPDM}}^{\text{max}}$  for  $L = 16$ ,  $V/J = 1$  and disorder strength  $W/J = 5, \dots, 15$ . The arrow denotes increasing disorder strength. For all values of  $W$ , a clear logarithmic growth with a non-universal prefactor is visible at long times. Inset: Comparison between  $\bar{S}_{\text{OPDM}}^{\text{max}}$  (full circles) and the von-Neumann entropy  $\bar{S}_{\text{vN}}$  (gray lines) for  $L = 16$ ,  $V/J = 1$  and  $W/J = 5, 15$ . Note that the prefactor of the logarithmic growth of the OPDM entropy and of the von Neumann entropy are different. (b) Same as in (a) for weak interactions  $V/J = 0.1$ .

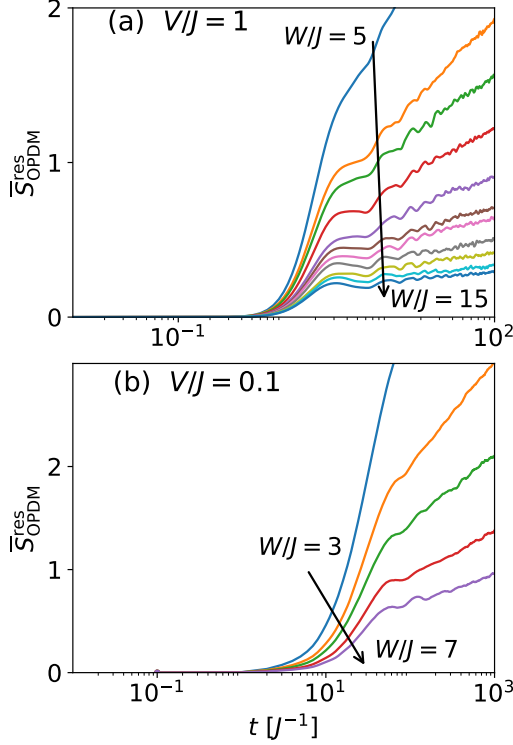


FIG. S3. (a): Main panel: Time evolution of the average residual OPDM entropy  $\bar{S}_{\text{OPDM}}^{\text{res}}$  for  $L = 16$ ,  $V/J = 1$  and disorder strength  $W/J = 5$ – $15$ . The arrow denotes increasing disorder strength. For all values of  $W$ , a clear logarithmic growth is visible. (b) Same as in (a) for weak interactions  $V/J = 0.1$ .

actions) with  $W/J = 5, \dots, 15$  in (a) and for  $V/J = 0.1$  with  $W/J = 3, \dots, 7$  (weak interactions) in (b). In both cases, the system is in the putative MBL phase. The quench protocol is the same as for  $\bar{S}_{\text{OPDM}}^{\text{min}}$  (see the main text). As is clear from the figure,  $\bar{S}_{\text{OPDM}}^{\text{max}}$  grows logarithmically with the time after the quench. In the insets of Fig. S2, we compare  $\bar{S}_{\text{OPDM}}^{\text{max}}$  and the von-Neumann entropy. Clearly, both entropies exhibit a logarithmic growth but with a different non-universal prefactor.

### S3. DYNAMICS OF FULL SYSTEM OPDM ENTROPY

It is interesting to consider the out-of-equilibrium dynamics of the OPDM entropy computed for  $A$  being the full system. Importantly, in the non-interacting limit, this entropy vanishes at any time, for any disorder realization, and for all eigenstates. This is not the case in the presence of interactions. For this reason, we refer to the OPDM entropy of the full system as “residual” entropy  $\bar{S}_{\text{OPDM}}^{\text{res}}$ . Here, we consider its disorder average  $\bar{S}_{\text{OPDM}}^{\text{res}}$ . Our results are reported in Fig. S3. In Figs. S3 (a) and (b), we plot  $\bar{S}_{\text{OPDM}}^{\text{res}}$  as a function of time for strong interactions and weak interactions, respectively. Remarkably, in all the cases, the data provide robust evidence that

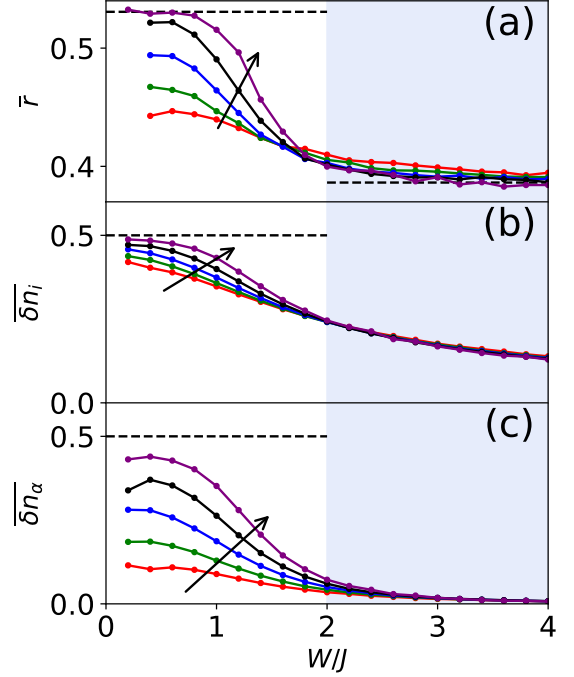


FIG. S4. Diagnostics of the MBL transition at  $V/J = 0.1$ : (a) average gap ratio  $\bar{r}$ , (b) average occupation distances  $\bar{\delta n}_i$ , (c) and  $\bar{\delta n}_\alpha$ .  $W/J$ , plotted on the horizontal axis is the disorder strength. We show data for for  $V/J = 0.1$ . Different curves corresponds to different system sizes  $L = 10, 12, 14, 16, 18$ . Data are averaged over up to  $10^5$  disorder realization. The arrow denote increasing system size. In (a), the horizontal dashed lines denote the analytic results assuming Wigner-Dyson ( $\bar{r} \approx 0.53$ ) and Poisson distribution ( $\bar{r} \approx 0.38$ ) of the energy spectrum. In (b), the occupation distances are expected to attain the values  $\bar{\delta n}_i = 1/2$  in the ergodic phase (dashed lines). In all panels, the shaded area is estimated to be in the MBL phase. Thus, all results shown in the main text are for disorder strength well above the transition.

$\bar{S}_{\text{OPDM}}^{\text{res}}$  increases logarithmically with time. This is interesting because it reveals how the logarithmic growth of the OPDM entropy (and of the entanglement entropy) in MBL phases is a genuine effect of the interactions.

### S4. MBL TRANSITION: ADDITIONAL NUMERICAL DATA FOR WEAK INTERACTIONS

In this section, we employ standard diagnostic tools to identify the putative MBL transition at  $V/J = 0.1$  (see the main text). Specifically, we consider the average gap ratio [35, 64] and the occupation distance measure [52].

We start discussing the average gap ratio  $\bar{r}$ . Given the eigenenergies  $E_i$  of the quantum many-body Hamiltonian, we first define the gaps  $\delta_n$  as

$$\delta_n \equiv E_{n+1} - E_n, \quad (\text{S.2})$$



The gap ratios  $r_n$  are defined as

$$0 \leq r_n \equiv \min\{\delta_n, \delta_{n-1}\} / \max\{\delta_n, \delta_{n-1}\} \leq 1. \quad (\text{S.3})$$

The average ratio  $\bar{r}$  results from averaging over the eigenstates of the Hamiltonian and over the disorder. For Poisson-distributed energy levels, i.e., for integrable systems, the average value of the ratio is  $\bar{r} = 2\ln(2) - 1 \approx 0.386$ . In the non-integrable case, one should expect that energy levels are described by the Gaussian Orthogonal Ensemble (GOE) [70]. This  $\bar{r} = 4 - 2\sqrt{3} \approx 0.535$  for  $3 \times 3$  matrices.

In Fig. S4 (a), we show  $\bar{r}$  [35, 64] as a function of  $W/J$ . The expected behavior [35, 64] is visible. At weak disorder,  $\bar{r}$  converges to the GOE result upon increasing  $L$ . On the other hand, in the strong-disorder regime  $\bar{r}$  is compatible with the Poisson value  $\bar{r} \approx 0.38$ . Using the scaling ansatz form  $\bar{r} = g(L^{1/\nu}(W - W_c))$  [35], with  $\nu$  a critical exponent and  $W_c$  the critical value of the disorder, we get  $W_c/J = 2.0(2)$  (we have used  $L = 14, 16, 18$  for the scaling collapse). However, similar to Ref. [35], one obtains  $\nu = 0.6(1)$ , which violates the Harris bound [56, 71, 72]. In conclusion, the analysis of the gap ratio  $\bar{r}$  suggests a change in behaviour at  $W_c/J \approx 2$ .

To complement our analysis, we also consider the occupation distances  $\delta n_i$  and  $\delta n_\alpha$  introduced in Ref. [52].

These are derived from the OPDM

$$\rho_{ij}^{(1)} = \langle \psi_n | c_i^\dagger c_j | \psi_n \rangle, \quad (\text{S.4})$$

where  $|\psi_n\rangle$  denotes an eigenstate. We define  $n_i$  as the fermionic spatial occupations  $n_i = \rho_{ii}$ , and  $n_\alpha$  are the eigenvalues of  $\rho_{ij}$ . Here, we consider the distances  $\delta n_i = n_i - [n_i]$  and  $\delta n_\alpha = n_\alpha - [n_\alpha]$  to the closest integers of  $[n_i]$  and  $[n_\alpha]$ , respectively. Finally, we obtain the averaged occupation distances  $\overline{\delta n_i}$  and  $\overline{\delta n_\alpha}$  by averaging over different disorder realizations.

The occupation distances measure the degree of Fock-space localization in the chosen single-particle basis. They are almost independent of system size in the MBL phase [52]. On the other hand, in the ergodic region,  $\overline{\delta n_i}$  must converge to the average particle filling, in our case 0.5, while  $\overline{\delta n_\alpha}$  approaches a smaller, energy-dependent value.

In Figs. S4(b) and (c), we plot the occupation distances  $\overline{\delta n_i}$  and  $\overline{\delta n_\alpha}$  as a function of  $W/J$ . We observe that  $\overline{\delta n_i}$  become almost  $L$ -independent for  $W/J > 2$ . For  $\overline{\delta n_\alpha}$ , this happens for  $W/J > 2.6$ . Thus, the occupation distances confirm the qualitative scenario obtained from the analysis of the gap ratio  $\bar{r}$  (see Fig. S4(a)).